Finite element modelling of transport in a tokamak edge and divertor.

Richard Marchand
Department of Physics, University of Alberta, Edmonton Alberta, T6G 2J1 Canada

Abstract
A finite element approach is described, for modelling transport in tokamak edge and divertor plasma. The method discretizes all transport equations on an unstructured triangular mesh. The advantages and difficulties of this approach are discussed. Results are presented and compared with experimental measurements made on TdeV. Example results are also given for JET, using a simplified physics model (single ion species, no neutrals and no flux limits), and using a more comprehensive model with helium impurity ions and neutrals.

1. Introduction
This letter presents a different approach to modelling the edge and divertor regions of tokamak plasmas from the ones generally in use. Plasma transport in tokamaks is almost universally modelled with a finite volume discretization on structured quadrilateral meshes[1-3]. While this method is well established and broadly adopted, it has some notable drawbacks and limitations. In particular, it doesn't lend itself naturally to an arbitrary SOL topology, it is limited in the ways in which the mesh may be refined, and the quadrilateral cells sometimes need to be highly stretched and twisted to accommodate divertor plates that are nearly tangent to the magnetic field lines. To be fair, this approach also has some strengths; the main ones being its relative simplicity, and its natural ability to accurately represent strong transport anisotropies in a magnetized plasma. In the following, the transport model and the discretization scheme are briefly described. Example simulations are then given for a pure deuterium plasma, and comparisons are presented with measurements made in the now decommissioned TdeV experiment. These comparisons focus on the H-alpha emissivity, the ion temperatures in the divertor and on the pumping efficiency of helium. Sample results are also presented for JET, for an idealized pure deuterium plasma, and for plasmas with a small concentration of helium.

2. Model description
A detailed description of the physical model and the numerical method used to solve the transport equations can be found in [4]. It is briefly summarized here for completeness. Transport of charged species is described in the fluid approximation. The equations for the conservation of particles, parallel momentum and energy are solved for every (positively charged) ionisation stage in the plasma. In addition, an equation is also solved for the conservation of electron thermal energy. Neutral particles transport is described in the diffusion approximation; that is, equations are solved for the conservation of neutral particles density and energy. In all cases, fluxes of neutral particles and energy are assumed to be purely diffusive, with a diffusion coefficient depending on the local collision and charge exchange mean free paths. Unless stated otherwise, all fluxes parallel to the magnetic field are classical, with a flux limit of 0.2. Uniform perpendicular diffusion coefficients are used to account for anomalous transport in the perpendicular direction. Boundary conditions are specified for the charged species densities and temperatures at the boundary between the SOL and the central region. At the divertor plates, the parallel velocity is

assumed to be equal to the local sound speed. Standard sheath boundary conditions are assumed for the electron and ion thermal fluxes at the plates. The parallel electron thermal energy flux there is taken to be $Q_{//e} = \delta_e n_e T_e C_s$, where C_s is the sound speed, and δ_e=5. A similar expression is used for the ion thermal energy flux at the plate, with δ_i=2.5. Finally, the effect of **E×B** drifts is always ignored. In practice, the inclusion of drift effects is found to have a large effect on the parallel velocity [4]. The other plasma profiles and net poloidal flows, however, are found to be relatively insensitive to the inclusion of drifts. The result is a set of several coupled nonlinear partial differential equations for the unknown variables. These are discretized in finite elements, using linear interpolation functions on an unstructured triangular mesh.

The development of this finite element approach was motivated by the following facts:
1) An unstructured mesh does not require any artificial cut in the at X point(s) as required when mapping a structured mesh onto a SOL. Once the model is developed for a given geometry, it is a straightforward exercise to extend it to other geometries with one or two X points, and boundaries (divertor plates) of arbitrary shapes. This applies to divertor, limiter or mixed configurations.
2) The problems associated with stretching and deformation of quadrilateral cells in the vicinity of divertor plates in notorious. This problem is absent with an unstructured grid. As a result, the construction of a suitable unstructured mesh is generally less problematic than that of a structured one.
3) Finally, a triangular unstructured mesh offers more flexibility for spatial refinement.

Figures 1 and 2 give examples of a structured and unstructured meshes calculated in the divertor region of JET. The issue of mesh refinement and spatial resolution is particularly obvious in the vicinity of the X point in both cases. For the structured mesh, the construction of a quasi-orthogonal mesh results in rather large cells at the X point being linked to (unnecessarily) small cells radially outward. In this case, increasing the resolution at the X point would imply even smaller cells away from it, where a finer resolution may not be needed. From Fig. 2, it is clear that mesh points may be added near the X point, and not affect the distribution of mesh points elsewhere. To be fair, a discretization based on an unstructured mesh comes with its own difficulties. Perhaps the most serious one is related with the necessity for strict alignment along the magnetic flux surfaces. This is required in order to preserve the strong anisotropy in electron thermal transport. It can indeed be demonstrated that, in order to avoid numerically corrupting the (week) anomalous perpendicular transport by the (much stronger) parallel transport, most cells must have a side that is parallel to the local magnetic field. In practice, this is achieved by requiring that the extremities of the aligned side be on the same magnetic field line. This actually imposes a serious constraint on the construction of unstructured meshes which, in their poloidal distribution, must be very similar to structured meshes. Alignment alone is, however, not sufficient to prevent corruption of perpendicular thermal diffusion by parallel transport. This can be understood by considering the following diffusive equation in which a diffusive flux only exists in the parallel direction, defined by the unit vector field **b**.

$$\frac{\partial T}{\partial t} - \nabla \cdot (\hat{b}\hat{b}\kappa \cdot \nabla T) = 0 \qquad (1)$$

If the unknown field is expressed as a superposition of linear interpolating functions N_j, if the resulting equation is multiplied by N_i and integrated over the entire domain, then, the second term in (1) yields, after an integration by parts,

$$\int d^2x\, \kappa(\nabla N_i \cdot \hat{b})(\nabla N_j \cdot \hat{b}) \qquad (2)$$

where the integration is carried over an element (a triangle). In order to ensure that this discretization does not lead to spurious transport in the perpendicular direction, it is necessary to ensure that the integral in (2) vanishes whenever nodes i and j are not on the same field line. By definition, a linear interpolating function N_i is equal to unity at node "i", it varies linearly in all elements connected to i, and it vanishes on all other nodes. Referring to Fig. 3, it follows that ∇N_i is perpendicular to the side opposite "i". Thus, if "i" and "j" correspond respectively to A and B in the figure; two nodes that are on different field lines, and the ingetral in (2) should vanish. For a curved field, and for finite size elements, this integral (and its numerical estimation) do not vanish exactly in general. The result is a spurious transport in the direction perpendicular to the field **b**. In the case of electron thermal diffusion, where the parallel diffusivity exceeds the (anomalous) perpendicular diffusivity by many orders of magnitudes, even a small non vanishing contribution from this integral will lead to a non acceptable corruption of perpendicular diffusion. For that reason, it is necessary to take some special action in assembling the global matrix (where integrals such as (2) are used) of the finite element formulation, to make sure that parallel thermal diffusion only couples nodes that are on the same field lines.

3. Results

In this section, simulation results are presented for representative TdeV operational conditions. Comparisons between simulation predictions and experimental measurements are made for the ion temperatures, for H-alpha emissivity and for helium enrichment in the pumping plenum. Results are also presented for JET; first with a very simple and idealized physics model, then with a more complete model.

3.1 D-alpha emissivity and ion temperatures in TdeV 95.

We first present some results obtained with the original TdeV divertor geometry, referred to here as TdeV 95. The results were obtained for discharge conditions corresponding to an intermediate density (line average density of approximately $3\times10^{19}m^{-3}$), at which partial detachment starts to be observed. These conditions are close to the ones analysed recently by Meo, et al. [5]. In this simulation, carbon impurities are taken into account. A small fraction (1%) of CV was assumed at the boundary with the central plasma. Carbon sputtering by DII is taken into account, with a fixed yield of 2%. Sputtering by other species (charged or neutral) is ignored. A 100% recycling coefficient is assumed for deuterium. All carbon fluxes incident on the plates are assumed to be totally absorbed. Figure 4 shows the D-alpha emissivity along the separatrix as a function of the vertical position, in the outer divertor region. This curve may be compared with the curves of maximum emissivity inferred in [5]. While the emissivity calculated here is of the same general

order of magnitude as that reported in [5], there are some noticeable differences. In particular, the simulated emissivity is systematically smaller, and it decreases towards the divertor plate. Part of these differences are probably attributable to the fact that, in [5], the emissivity plotted is along the path of maximum emissivity, while Fig. 4 shows the emissivity along the separatrix. Yet, the region of maximum emissivity in Tdev95 is known to be slightly outside the separatrix, and the distance between this maximum and the separatrix increases as the distance to the divertor plate decreases.

Another calculation of interest is the ion temperatures for DII and the first three ionisation stages of carbon. These temperatures, calculated along the separatrix in the outer divertor region, are plotted in Fig. 5. The first thing to note is that not all ion species have the same temperature. Indeed, CII has a significantly lower temperature close to the divertor plate, where it is generated from the ionisation of 'cold' carbon neutrals, and where charge-exchange cooling is significant. The temperatures of the higher ionisation stages are larger, and nearly equal to that of DII, with CIV being the closest. This faster equilibration of the higher ionisation stages with DII is an obvious consequence of fast increase of the collision frequency with ion charges. We conclude from these results that, for practical purpose, the single ion temperature approximation is excellent for the higher ionisation stages. Singly ionised ions, however, can probably not be modelled with the same temperature as the bulk ions. At least close to the divertor plates (where their density is significant), they probably require to be described with their own temperature or, possibly, with kinetic theory. Finally, the computed DII temperature profile can be compared with the ones in Fig. 13 of [5]. The simulated profile here is seen to be closer to the 'calculated' profile quoted in [5], than to the one obtained from the onion skin model. In particular, the DII temperature profile shown in Fig. 5 exhibits a significant gradient near the plate, comparable to the 'calculated' profile in [5].

3.2 Helium enrichment in TdeV 96.

Helium enrichment η in the pumping plenum of TdeV has been measured experimentally for two configurations [6] in the last divertor geometry of TdeV. In one, the entrance to the pumping plenum is through the private region (Inboard Pumping) while, in the other (Fig. 6), it is through the SOL (Outboard pumping). Experimentally, He enrichment was defined as the ratio of helium to deuterium neutral density in the pumping plenum, divided by the ratio of helium to deuterium ion densities in the central plasma. In the simulations, enrichment is defined as the ratio of neutral helium flux to the deuterium flux at the entrance of the pumping plenum, divided by the ratio of the helium density to the deuterium density at the boundary between the SOL and the core region. Referring to Fig. 2 of [6], the outboard pumping configuration considered here corresponds to the middle configuration, while the inboard configuration corresponds to the one on the right. A comparison between simulated and measured enrichments is given in Fig. 7. The two definitions of enrichment are not strictly the same, which accounts for some of the discrepancies. Nonetheless, there is qualitative agreement in that both the measured and the computed enrichment are seen to be a decreasing function of density. Moreover, the rate at which η decreases with density tends to decrease in all cases, as density increases.

A comparison of η predicted with B2-EIRENE simulations is reported in [6]. These results, not reproduced here, are systematically smaller than the measured values; typically by a factor two to four. Here again, quantitative differences may be explained, in part, by the different definition of η in the model and in the experiment. Perhaps more significantly, the tendency of η predicted with B2-EIRENE seems to be qualitatively different from the one determined experimentally. Indeed, the simulated enrichment factor reported in [6] is not a monotonically decreasing function of the density. For both inboard and outboard pumping configurations, η is predicted to be a decreasing function of density at low density and an increasing one at higher density.

3.3 Example simulation with JET: simplified physics model

Simulations have been done for the JET geometry with a greatly simplified physics model. In these, particle recycling and the presence of neutral species is ignored, and all flux limits are turned off. The purpose of such a simulation is to facilitate an eventual comparison with other numerical approaches by presenting results that will depend more on the specific numerical methods, rather than on the physics. The mesh used in the simulations is illustrated in Fig. 2, for the vicinity of the divertor region. The innermost flux surface in the midplane (z=0.393m) extends to R=3.824m. In that plane, the separatrix extends to R=3.858 and the outermost flux surface, to R=3.890. The density assumed at the boundary with the central region is $10^{19}m^{-3}$, and the temperature there is 200eV. This, at steady state, yields an input power of approximately 1.2 MW from the core to the SOL. Of that, 60% is deposited on the outer divertor plate, and 40%, on the inner plate. The resulting electron density profile is shown in Fig. 8. It is, of course, not possible to compare the results obtained in this approximation with experiment. They are presented to illustrate the type of comparison that would be possible with other calculations.

3.4 Example simulation with JET: more representative plasma conditions

Figures 9 and 10 illustrate some simulation results obtained with the more complete physics model described in Sec. 2. The conditions imposed for the deuterium density and temperature at the boundary with the central plasma are the same as in 3.2. The main difference here is that flux limiters with f=0.2 are used in all (otherwise classical) parallel fluxes. At the boundary with the centre, a fixed density ratio of 10% is assumed between helium and deuterium; that is, the helium density is assumed to be $10^{18}m^{-3}$ there. The helium temperature at that boundary is assumed to be 200eV, as for the other species. Plasma sputtering at the divertor plates is neglected, but both deuterium and helium are assumed to recycle with 100% efficiency. A comparison of Figs. 9 with 8 shows the effect of the simplifications made in 3.2. The effect of recycling as a source of plasma is obvious from this comparison. The plasma density calculated in the divertor is significantly larger, and the profile is qualitatively different when recycling and neutral ionisation are taken into account. Finally, Fig. 10 shows the calculated two dimensional distribution of neutral helium density. This figure indicates that the highest concentration of HeI is on the divertor plates, very close to the strike point with the separatrix.

4. Summary and conclusion

In summary, a comprehensive two dimensional model has been developed to simulate transport in tokamak edge and divertor regions. This model uses a numerical approach that is different from the one used generally in other models. This alternative approach has the advantage of allowing more flexibility in defining the spatial mesh resolution. Because it uses a triangular unstructured grid, it is free of the problems associated with stretched and deformed cells at divertor boundaries, when the magnetic field is nearly tangent to the plates. It is also readily applicable to a broader class of magnetic field configurations including divertor, limiter, or mixed configurations. Results have have been obtained, that are in reasonable agreement with measurements made on TdeV. An interesting feature of the model is that it allows for as many ion temperatures as there are ion species. Simulations made for TdeV indicate that the single ion temperature approximation, used in other transport models, is indeed a good approximation for all charged species, except for the lower impurity ionisation stage(s). In the divertor region, these species are affected by a strong ionisation source of cold ions and by charge exchange with 'cold' neutrals. As a result, their temperature is significantly lower than that of the bulk ions. A proper description of these species thus requires, at least, a separate ion energy equation. In instances when very different ion temperatures would be predicted, or temperatures with strong parallel gradients, a kinetic description of the ion species may even be required.

Acknowledgement
Thanks to Alberto Loarte and Andrei Kukushkin for kindly providing JET equilibrium and structure files. I am grateful to J.-L. Gauvreau for some e-mail exchanges concerning helium enrichment measurements in TdeV. This work made use of the Multimedia Advanced Computational Infrastructure (MACI) jointly supported by the Canada Fund for Innovation and by the Alberta Innovation and Science Research Investment Program. This work was supported by the Natural Sciences and Engineering Council of Canada.

References

1. R. Schneider, et al., J. Nucl. Mater. 220-222, 1076 (1995).
2. A. Taroni, et al., J. Nucl. Mater. 220-222, 400 (1995).
3. G.R. Smith, et al., J. Nucl. Mater. 220-222, 1024 (1995).
4. R. Marchand and M. Simard, Nucl. Fusion 37, 1629 (1997).
5. F. Meo, et al., Phys. Plasmas 7, 2494 (2000).
6. J.-L. Gauvreau, et al., J. Nucl. Mat 266-269, 307 (1999).

Figure captions

Fig. 1. Illustration of a structured quadrilateral mesh computed for JET, in the divertor region.

Fig. 2. Illustration of a triangular unstructured mesh computed for JET, in the divertor region.

Fig. 3. Illustration of an ‘aligned’ triangular element in the presence of curved magnetic surfaces.

Fig. 4. D-alpha emissivity along the separatrix between the X point (lower Z value) and the divertor plate (higher Z value) in the outer divertor region, as a function of the vertical position Z. The emissivity is in units of 10^{21} photons radiated per second, per cubic metre. For reference, the divertor plate is located at Z=0.44.

Fig. 5. Ion temperature profiles calculated for DII, CII, CIII and CIV between the X point and the divertor plate, along the separatrix, in the outer divertor region, as in Fig. 1. For reference, the divertor plate is located at Z=0.44.

Fig. 6. Illustration of the Outboard Pumping configuration in TdeV. In this equilibrium, the separatrix intersects the upper divertor plate and the entrance to the pumping plenum is through the SOL. In the inboard pumping configuration, the separatrix intersects the lower (oblique) divertor plate. In that case, entrance to the pumping plenum is through the private region.

Fig. 7. Comparison between the measured and simulated helium enrichment at the entrance of the pumping plenum in TdeV, for inboard (I) pumping and outboard (O) pumping.

Fig. 8. Two dimensional electron density profile computed for JET with the reduced physics model.

Fig. 9. Two dimensional electron density profile computed for JET with the more complete physics model.

Fig. 10. Two dimensional neutral helium density profile computed for JET with the more complete physics model.

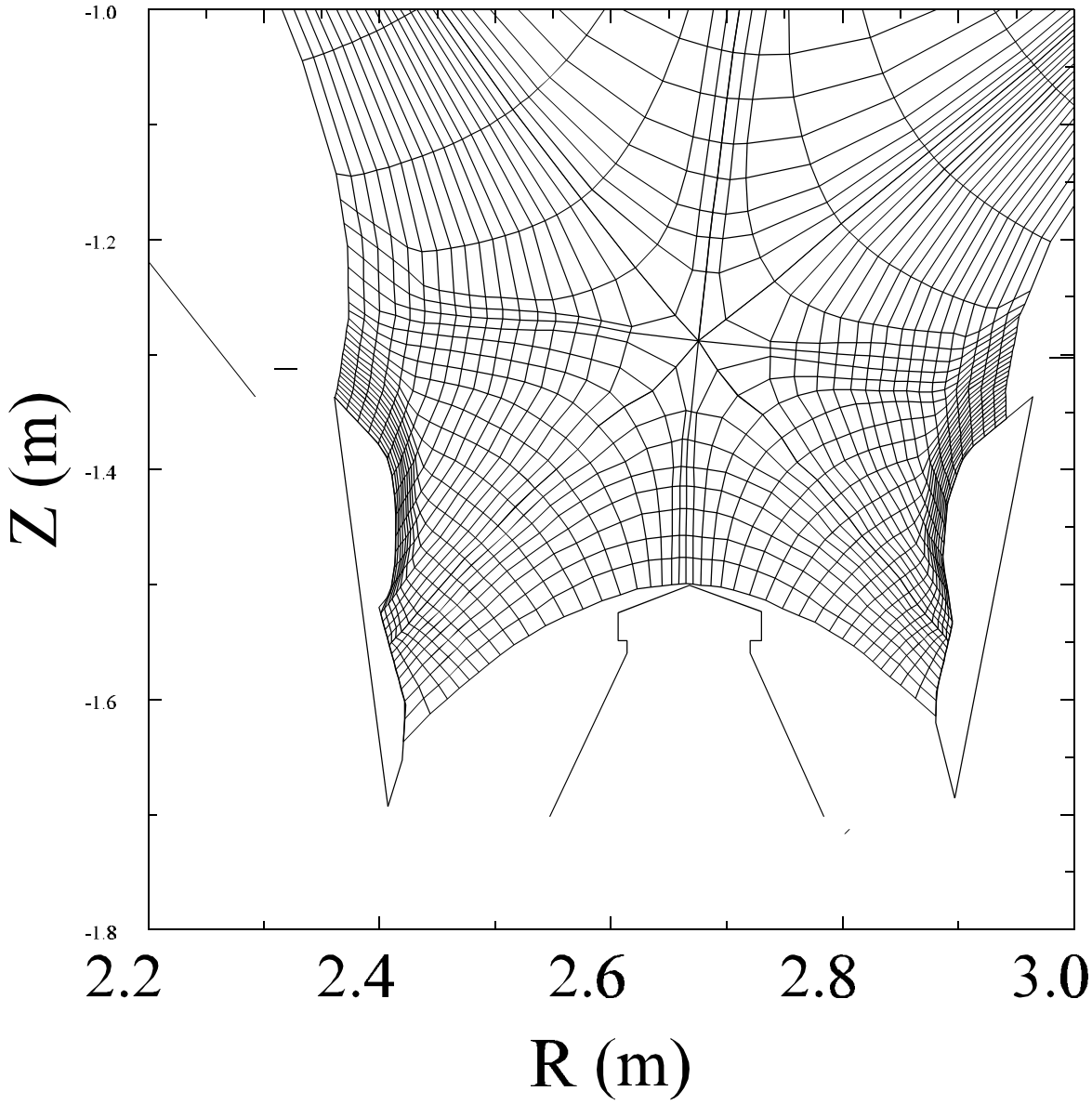

Figure 1.

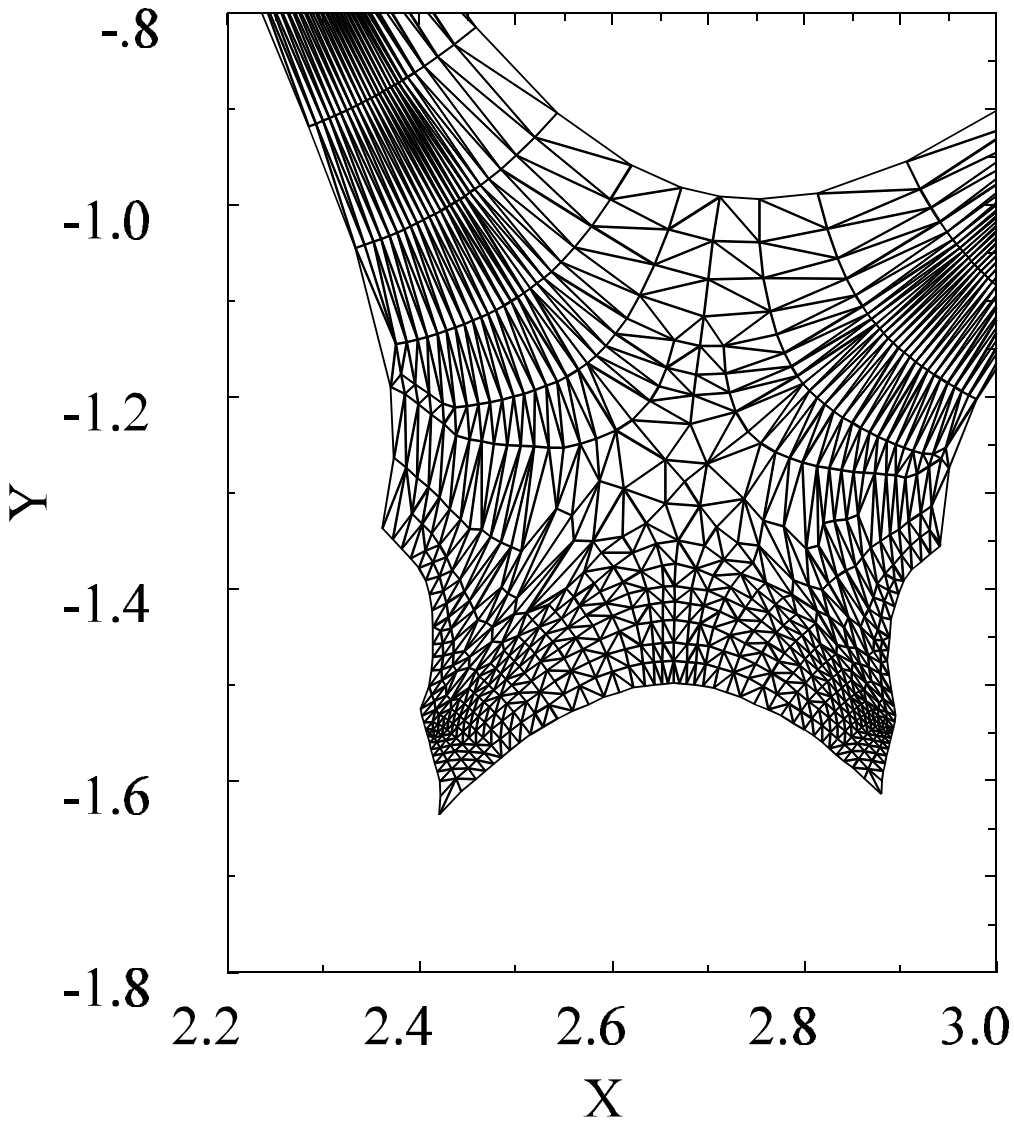

Figure 2.

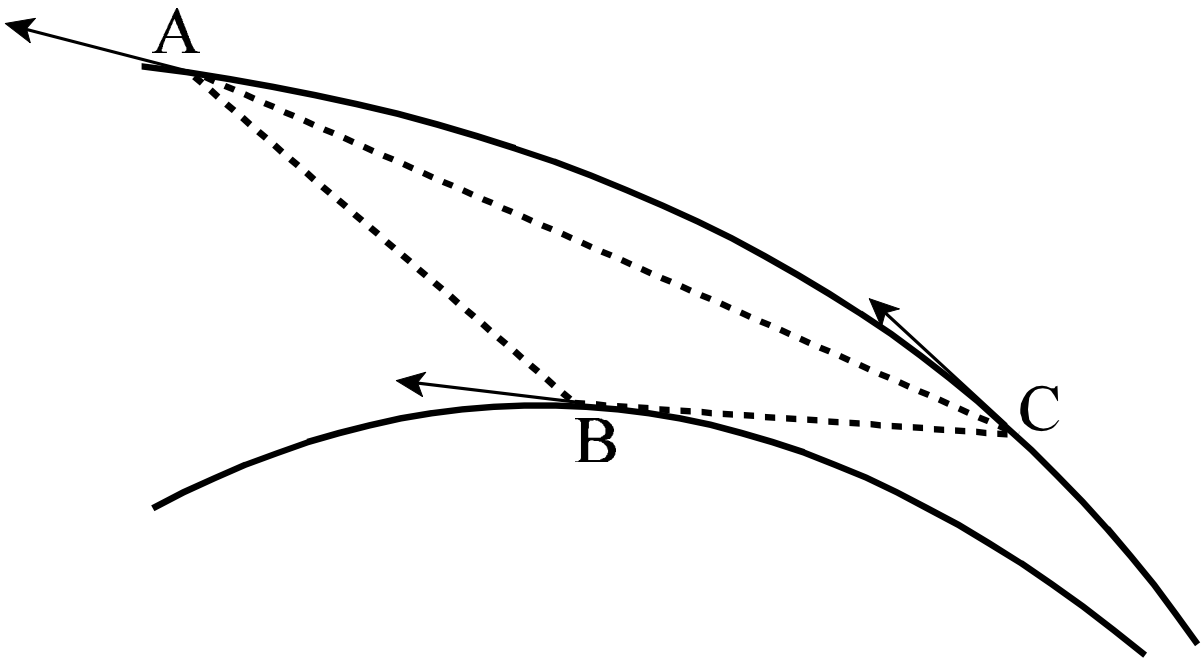

Figure 3.

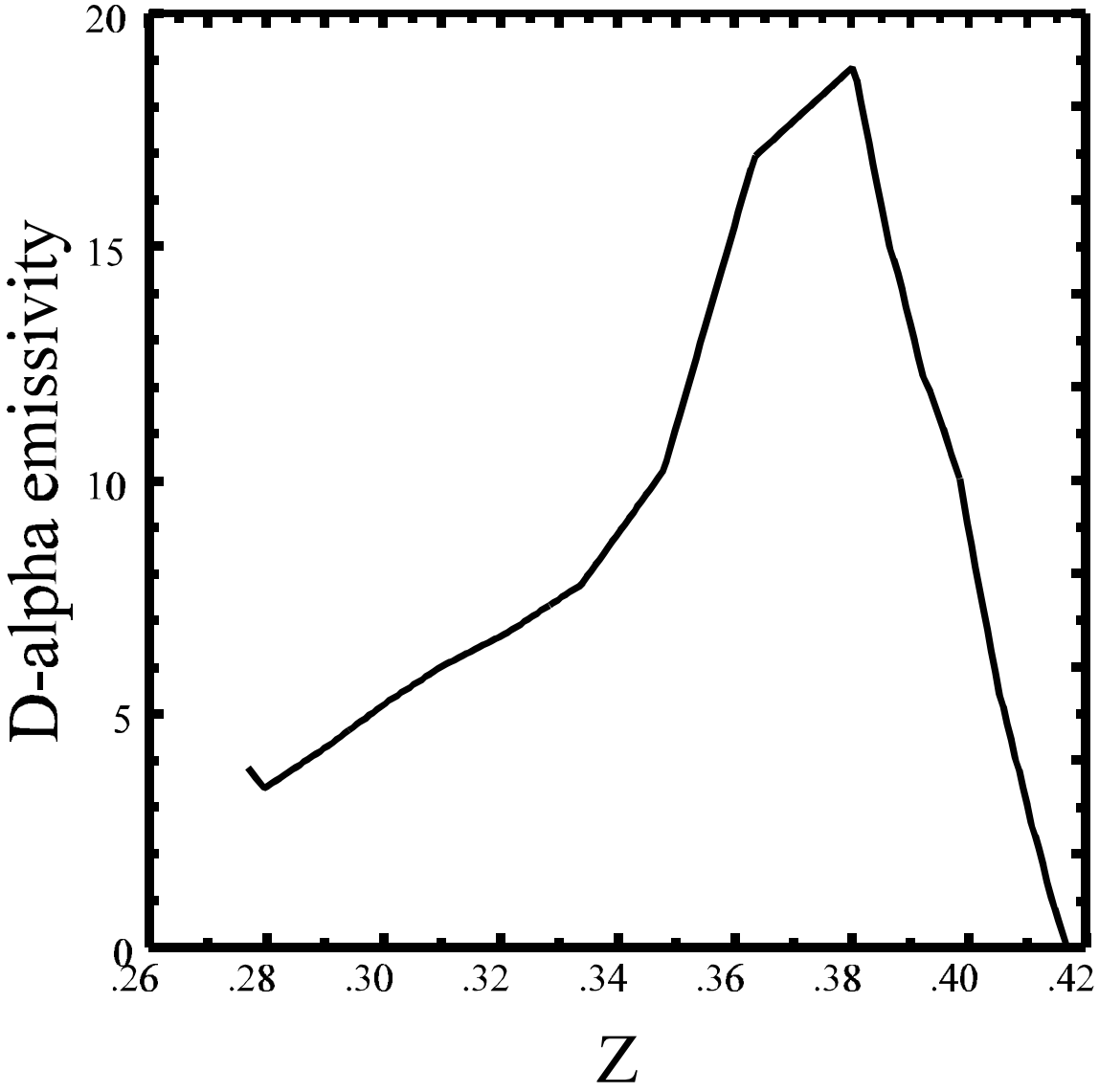

Figure 4.

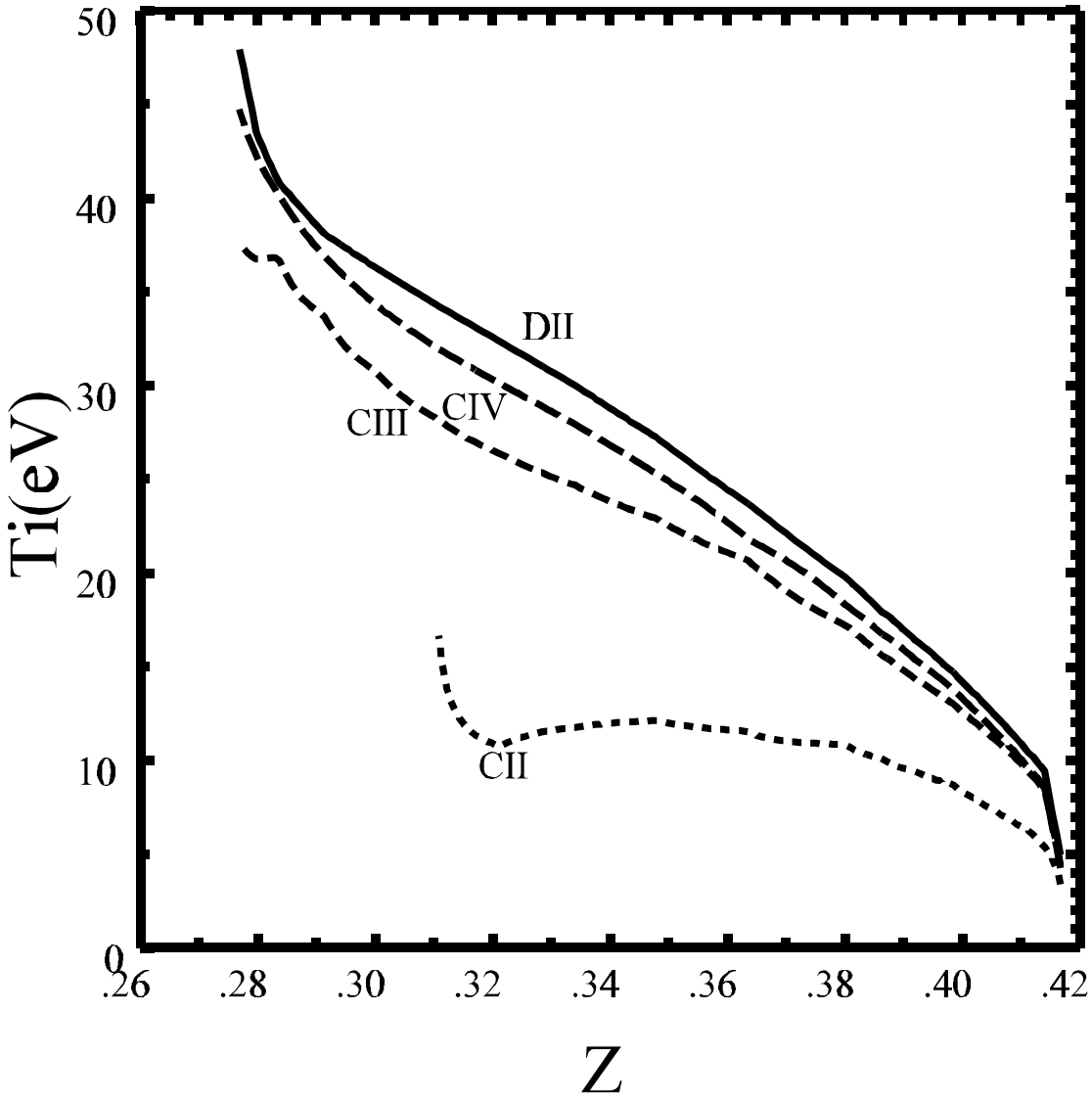

Figure 5.

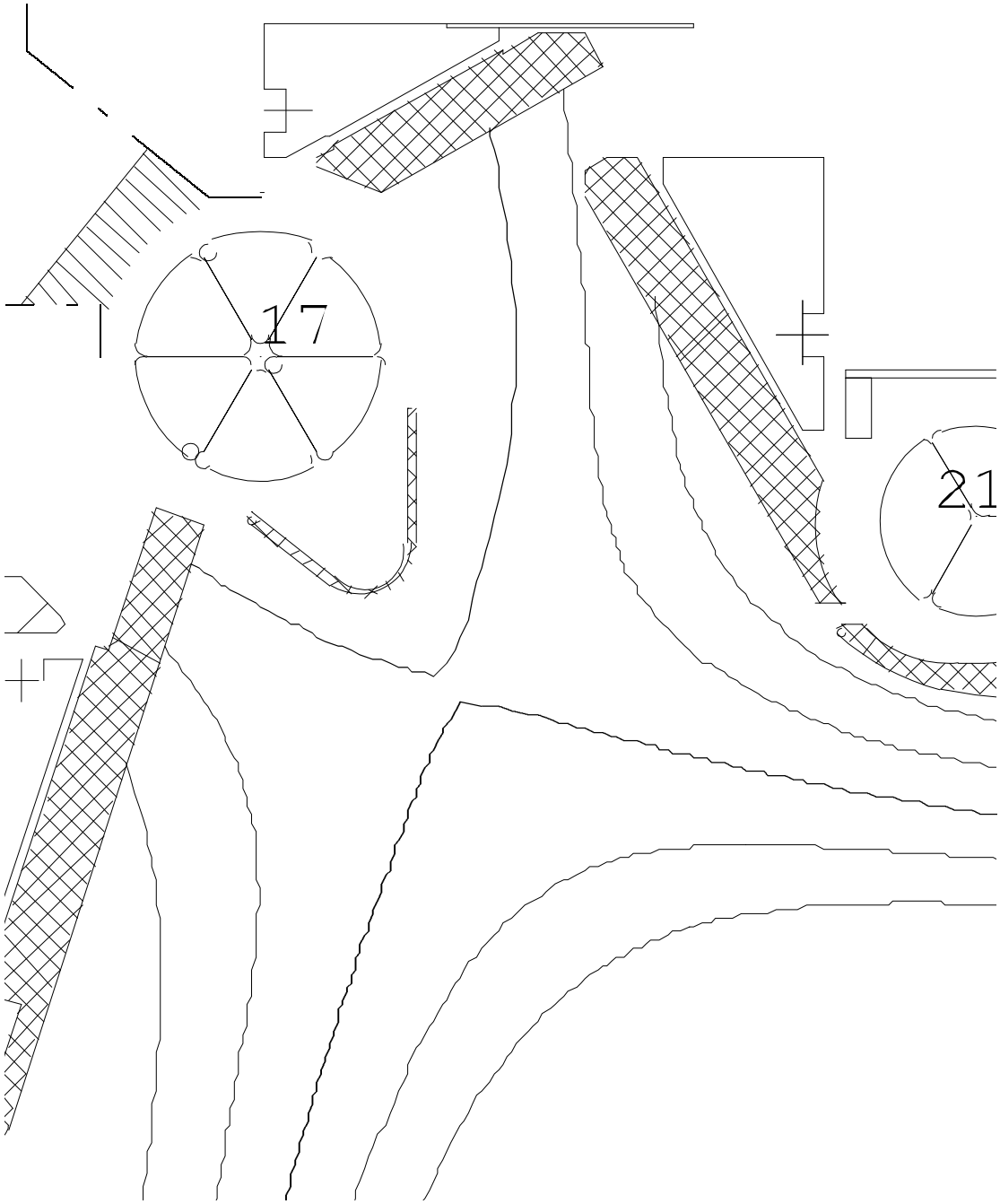

Figure 6.

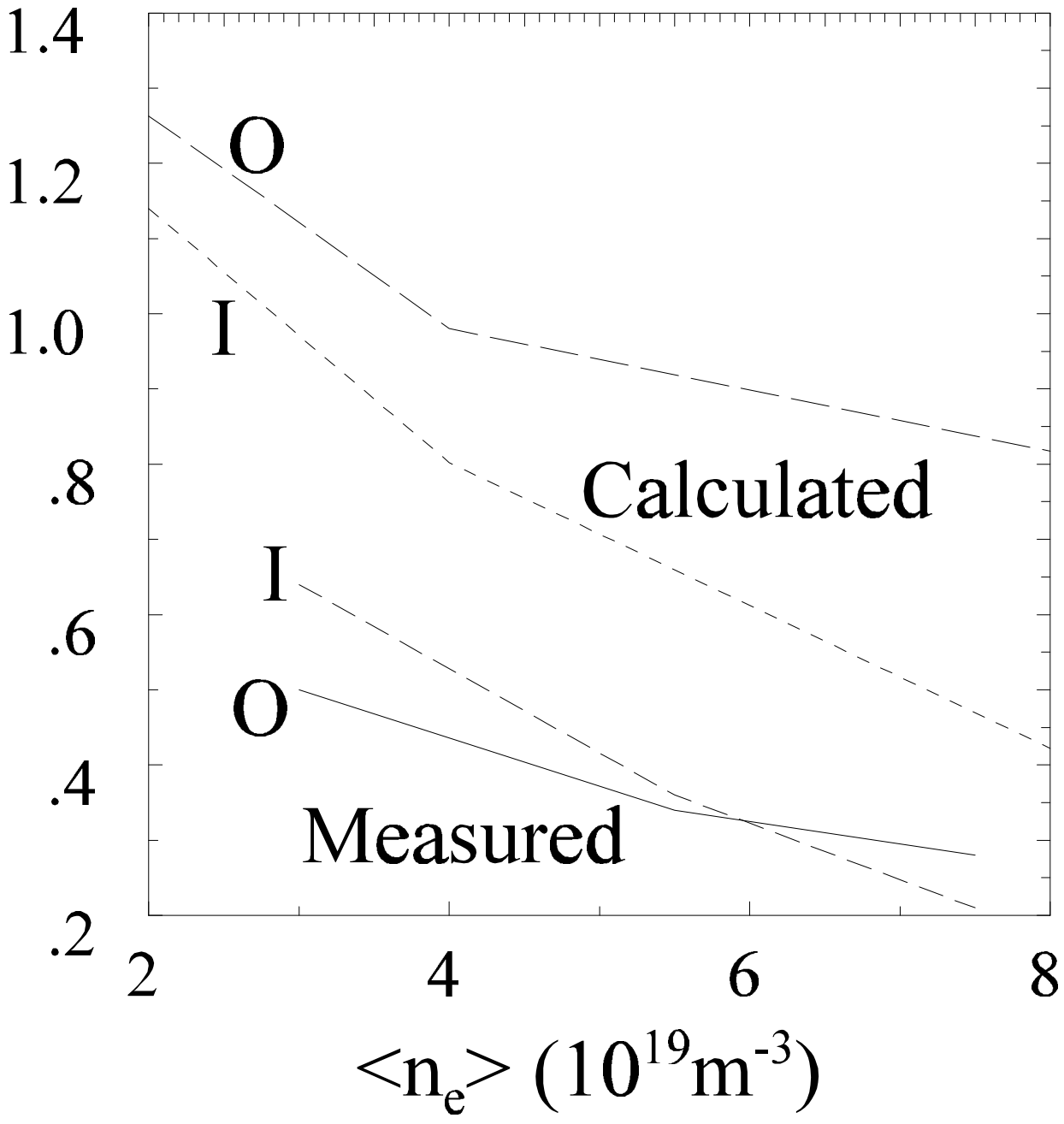

Figure 7.

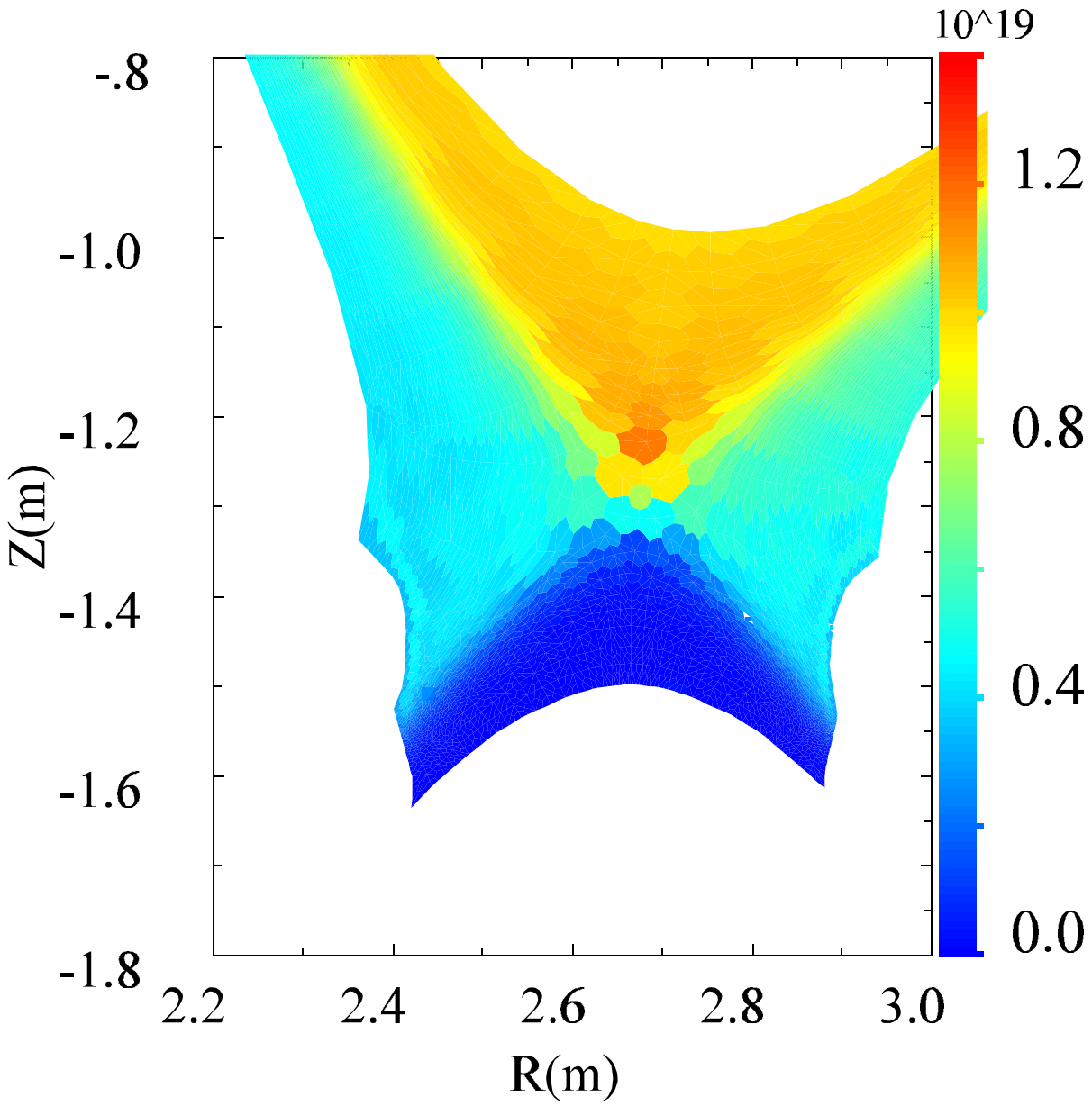

Figure 8.

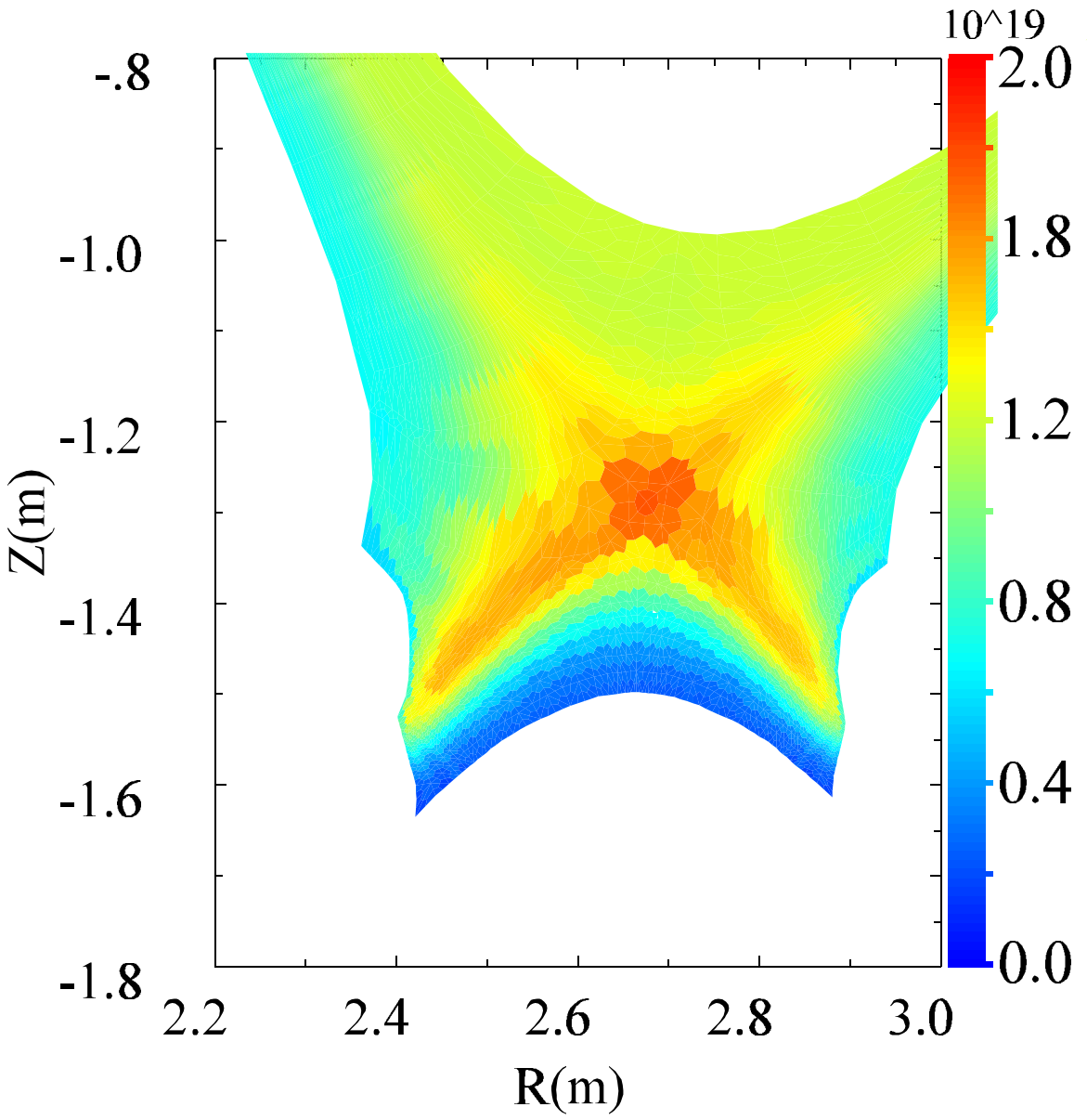

Figure 9.

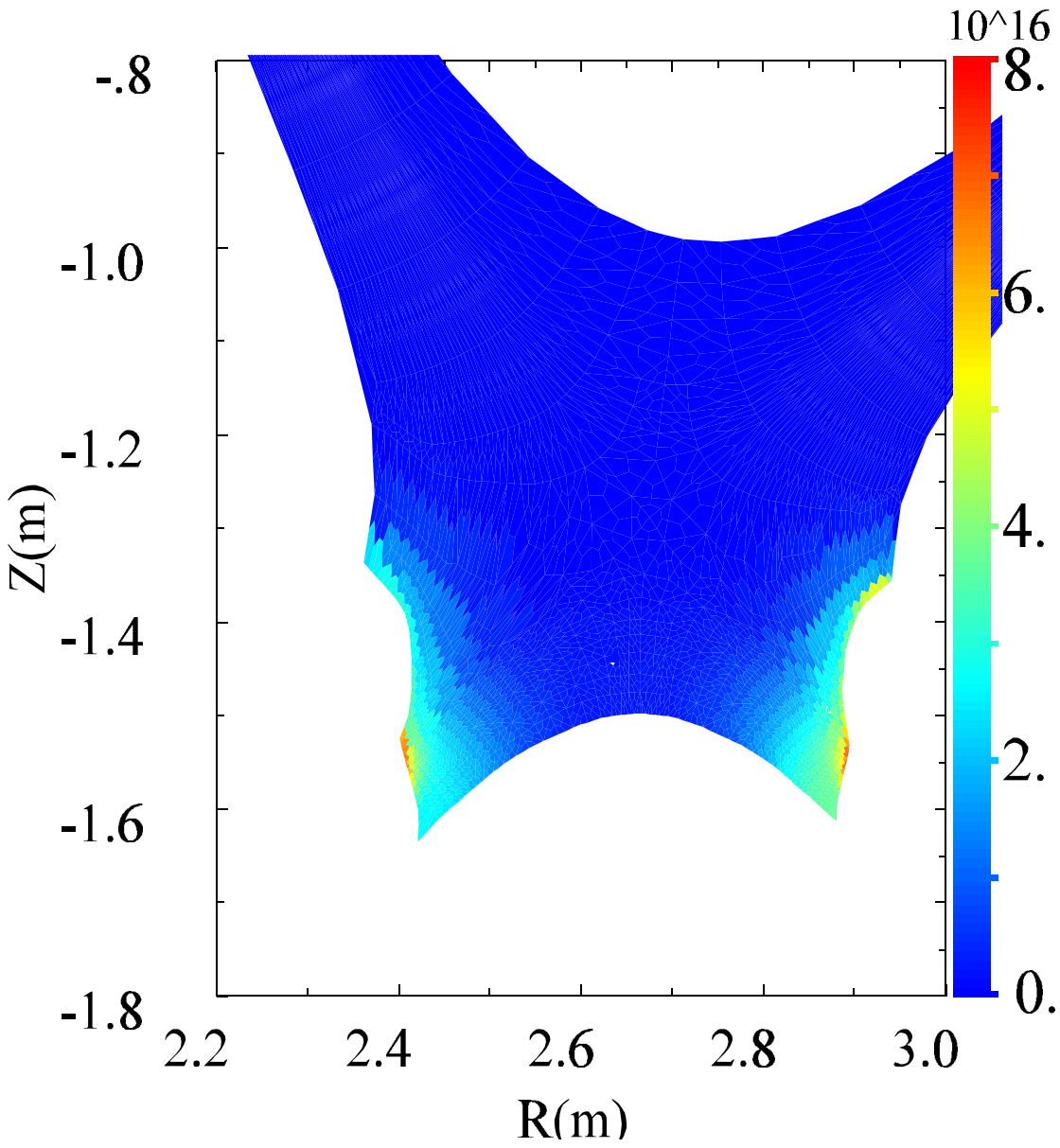

Figure 10.